

Tachyonic instability of the scalar mode prior to QCD critical point based on Functional renormalization-group method

Takeru Yokota* and Teiji Kunihiro†

Department of Physics, Faculty of Science, Kyoto University, Kyoto 606-8502, Japan

Kenji Morita‡

Yukawa Institute for Theoretical Physics, Kyoto University, Kyoto 606-8502, Japan

Institute of Theoretical Physics, University of Wrocław, PL-50204, Wrocław, Poland

We establish and elucidate the physical meaning of the appearance of an acausal mode in the sigma mesonic channel, found in the previous work by the present authors, when the system approaches the Z_2 critical point. The functional renormalization group method is applied to the two-flavor quark-meson model with varying current quark mass m_q even away from the physical value at which the pion mass is reproduced. We first determine the whole phase structure in the three-dimensional space (T, μ, m_q) consisting of temperature T , quark chemical potential μ and m_q , with the tricritical point, $O(4)$ and Z_2 critical lines being located; they altogether make a wing-like shape quite reminiscent of those known in the condensed matters with a tricritical point. We then calculate the spectral functions $\rho_{\sigma,\pi}(\omega, p)$ in the scalar and pseudoscalar channel around the critical points. We find that the sigma mesonic mode becomes tachyonic with a superluminal velocity at finite momenta before the system reaches the Z_2 point from the lower density, even for m_q smaller than the physical value. One of the possible implications of the appearance of such a tachyonic mode at finite momenta is that the assumed equilibrium state with a uniform chiral condensate is unstable toward a state with an inhomogeneous σ condensate. No such an anomalous behavior is found in the pseudoscalar channel. We find that the σ -to- 2σ coupling due to finite m_q play an essential role for the drastic modification of the spectral function.

I. INTRODUCTION

It is expected that hot and dense matter as described by the quantum chromodynamics (QCD) shows a rich phase structure and the nature of the phase transitions as well as the phase structure itself depends on the external parameters such as temperature T , quark chemical potential μ , isospin chemical potential μ_I and so on. Furthermore, their current quark-mass dependence adds interesting complications, which in turn provide us with a theoretical clue to understand the mechanism of the QCD phase transitions. For vanishing chemical potential, the celebrated Columbia plot [1] shows us how the nature of the phase transitions may change along with that in the current quark masses. At finite μ and T , the change of the phase structure along with that of the current quark masses is expected as follows. For simplicity, we shall take the two-flavor case composed of u and d quarks and assume that $U_A(1)$ is kept broken at the chiral phase transition¹. In the chiral limit, an $O(4)$ critical line will exist in the small μ region in accordance with the Columbia plot. In the case of the physical quark masses, it is considered that there appears a *first-order* phase transition line in the large- μ and low- T region while the phase change becomes crossover in the small- μ and high- T region [5–7]. The endpoint of the first-order phase transition line is of a *second order* one and belongs to the same universality class as that of the 3D Ising model and is called a Z_2 critical point: Indeed

the current quark mass m_q plays the much the same role as the external magnetic field in the Ising model, which can take positive and negative values. The Z_2 critical point moves as m_q is varied and its trajectory constitutes the Z_2 critical lines in the three-dimensional (T, μ, m_q) -space with fictitious negative m_q axis being included. Thus the $O(4)$ critical line bifurcates at some μ into the two Z_2 critical lines existing both in the positive and negative m_q region resulting a wing-like structure [8]; such a bifurcation point or the endpoint of the $O(4)$ critical line is called a tricritical point, and a similar structure appears in various systems including metamagnets and ^3He - ^4He mixtures [9, 10].

One of the characteristics of any critical point is the existence of soft modes. It is also the case with the $O(4)$ and the Z_2 critical points: In the chiral limit, the sigma meson must be massless as are the three pions at the $O(4)$ critical point because of the $O(4)$ symmetry. Accordingly the soft modes composed of the pions and the sigma meson form a quartet at the $O(4)$ critical point. In contrast, the nature of the soft modes on the Z_2 critical line is somewhat involved: The charge conjugation symmetry is broken due to a finite μ , in addition to the chiral symmetry owing to the finite quark masses irrespective of current or dynamical ones. This gives rise to a nonvanishing coupling between the fluctuations in Lorentz-scalar and (the zero-th component of) vector channels, i.e., the baryon number susceptibility [11], which should become divergent on the Z_2 critical line [12]². Thus it is argued [13, 14] that the soft mode at the Z_2 critical point is

* tyokota@ruby.scphys.kyoto-u.ac.jp

† kunihiro@ruby.scphys.kyoto-u.ac.jp

‡ kmorita@yukawa.kyoto-u.ac.jp

¹ There has been a debate on the fate of $U_A(1)$ symmetry at high temperature since Ref. [2], though it is beyond our scope in this paper. See, e.g., [3, 4] and references therein for recent developments.

² Precisely speaking, the energy fluctuation can be also coupled to these quantities, but the incorporation of the energy fluctuation is beyond the scope of the present work.

mainly composed of the particle-hole (p-h) modes describing density fluctuations or hydrodynamic modes in the isoscalar channel while the mesonic mode mainly composed of the σ becomes a hard mode³. These analyses were based on the random phase approximation (RPA) of the Nambu–Jona-Lasinio model, the time-dependent Ginzburg–Landau theory [13] and the Langevin equation consisting solely of the slow variables in the vicinity of the critical point [14].

Although the above analyses should be true at least in the very vicinity of the Z_2 critical point, the problem is how large is the critical region itself. For a determination of the critical region, an analysis is necessary which incorporates other modes than the soft modes and their mutual couplings systematically. In the previous work [15], the present authors investigated the spectral properties of the low-energy modes near a Z_2 critical point using the functional renormalization group (FRG) method, which is one of the non-perturbative methods of the field theory [16–18]. In Ref. [15], the quark–meson model was employed as the bare action where the parameters including the current quark mass were chosen so that the physical quantities such as the pion mass are reproduced. It means that a special point on the Z_2 critical line was exclusively investigated. The spectral function $\rho_{\sigma,\pi}(\omega, p)$ in the scalar and pseudo-scalar channels were calculated, and the dispersion relations of the mesonic and p-h modes were also extracted from the ridge of $\rho_{\sigma,\pi}(\omega, p)$: It was confirmed that the p-h phonon mode in the sigma channel certainly behaves as the genuine soft mode in the very vicinity of the Z_2 critical point. A surprise was that the dispersion curve $\omega_{\sigma}(p)$ which is extracted as the ridge of $\rho_{\sigma}(\omega, p)$ once sitting in the time-like region penetrates into the space-like region with small and vanishing momenta as the system approaches the critical point but still before the phonon mode acquires the nature of the soft mode. A notable point is that such an anomalous behavior necessarily leads to a superluminal group velocity of the mode, implying the appearance of the tachyonic mode. The system with Z_2 critical point is characterized by the explicit violation of the chiral symmetry and the charge conjugation symmetry due to finite m_q and μ , which in turn induce the couplings of the sigma with 2σ and p-h excitation modes, respectively. Thus the appearance and absence of the anomalous behavior of the sigma mode mentioned above should be affected crucially by the values of m_q and μ .

In the present work, we shall investigate the behavior of the low-energy modes around the Z_2 critical point by varying the current quark mass, and thereby establish and elucidate the physical meaning of the anomalous behavior of the sigma-mesonic mode. As in the previous work, we calculate the thermodynamic quantities and the spectral functions in the mesonic channels using the FRG method with the 2-flavor quark–meson model. We first give a complete determination of the phase structure in the (T, μ, m_q) -space with the tricritical point, O(4) and Z_2 critical lines being located;

the resultant phase diagram makes a wing-like shape which is quite reminiscent of those known in the condensed matters with a tricritical point, such as metamagnets and ^3He – ^4He mixtures. It is then confirmed that the σ meson is the soft mode of the O(4) critical point in the chiral limit in the sense that the σ mass tends to vanish as the system approaches the critical point. Then it is shown for finite m_q that the σ mesonic mode becomes superluminal at finite momenta before the system reaches the Z_2 point from the lower density even for m_q finite but smaller than the physical value. We argue that the appearance of such a tachyonic mode with a superluminal velocity at finite momenta may imply that the assumed equilibrium state with a uniform chiral condensate is unstable for a phase transition toward a state with an inhomogeneous σ condensate. We confirm that such a drastic change of the spectral properties in the σ channel is attributed to the σ -to- 2σ coupling due to finite m_q .

The paper is organized as follows. In Sec. II, we give a brief description of the FRG method and the bare action. The parameter setting and the values of the current quark mass used in our calculation are presented in Sec. III A. In Sec. III B, we give a complete phase diagram in the (T, μ, m_q) -space with the locations of the O(4) and the Z_2 critical lines, which makes a wing-like structure. In Sec. III C, we show the results of the spectral functions in the mesonic channels near the critical points on the O(4) critical line and the Z_2 critical line and discuss the behavior of the low-energy modes as the current quark mass is varied. Section IV is devoted to a summary.

II. FORMULATION

In this section, we briefly outline the method which was developed in Refs. [19, 20] for the mesonic spectral functions based on the functional renormalization group. More details can be found in Ref. [15].

In the functional renormalization group (FRG) method, the effective average action (EAA) Γ_k , which depends on the momentum scale k , is introduced. The scale dependence of EAA follows the exact functional flow equation [21]:

$$\partial_k \Gamma_k[\Phi] = \frac{1}{2} \text{STr} \left[\frac{\partial_k R_k}{\Gamma_k^{(2)}[\Phi] + R_k} \right]. \quad (1)$$

Here, Φ represents all fields in the model including bosons and fermions, and $\Gamma_k^{(n)}[\Phi] := \delta^n \Gamma_k / \delta \Phi^n$ (n is a natural number). R_k is a regulator function which suppresses propagations of lower momentum modes than k . The flow starts at large UV scale $k = \Lambda$, where EAA becomes the bare action, and ends at IR scale $k \rightarrow 0$, where all the quantum fluctuations are incorporated and hence EAA becomes the effective action. Physical quantities are derived from the solution $\Gamma_{k \rightarrow 0}$ of Eq. (1).

To explore physics around the QCD critical point, we employ the two-flavor quark–meson model which is a chiral effective model of low-energy QCD. The bare action at finite temperature (T) and finite quark chemical potential (μ) in the

³ One notes that the spectral functions $\rho_{\text{ph}}(\omega, p)$ of the p-h modes have a support in the space-like region ($\omega < p$) while the mesonic one in the time-like region ($\omega > p$)

imaginary-time formalism is given by:

$$S_\Lambda [\bar{\psi}, \psi, \phi] = \int_0^{\frac{1}{T}} d\tau \int d^3x \left\{ \bar{\psi} (\not{\partial} + g_s(\sigma + i\vec{\pi} \cdot \vec{\pi}\gamma_5) - \mu\gamma_0) \psi + \frac{1}{2}(\partial_\mu\phi)^2 + U_\Lambda(\phi^2) - c\sigma \right\}. \quad (2)$$

Here, $\phi = (\sigma, \vec{\pi})$ denotes the chiral O(4) multiplet and σ and $\vec{\pi}$ represent the σ and π meson fields, respectively. The quark field ψ has the indices of the flavor $N_f = 2$ and the color $N_c = 3$. The quarks are coupled with the mesonic fields through the Yukawa coupling whose strength is represented as g_s . $U_\Lambda(\phi^2)$ is the potential term of the mesons. The last term $-c\sigma$ corresponds to the nonzero current quark mass thus explicitly breaks the $N_f = 2$ chiral symmetry when $c \neq 0$.

Our purpose is to calculate the mesonic spectral functions $\rho_{\sigma(\pi)}$, which can be obtained from the imaginary parts of the retarded Green's functions $G_{\sigma(\pi)}^R$:

$$\rho_{\sigma(\pi)}(\omega, \vec{p}) = -\frac{1}{\pi} \text{Im} G_{\sigma(\pi)}^R(\omega, \vec{p}). \quad (3)$$

In the imaginary-time formalism, the retarded Green's functions can be derived from the analytic continuations of the temperature Green's functions [22].

We define the scale-dependent temperature Green's functions $\mathcal{G}_{k,\sigma(\pi)}(P)$ for the sigma and the pion with isovector index a as follows:

$$\frac{\delta^2 \Gamma_k}{\delta \sigma(P) \delta \sigma(Q)} \Big|_{\Phi=\Phi_0} = (2\pi)^4 \delta(P+Q) \mathcal{G}_{k,\sigma}^{-1}(P), \quad (4)$$

$$\frac{\delta^2 \Gamma_k}{\delta \pi^a(P) \delta \pi^a(Q)} \Big|_{\Phi=\Phi_0} = (2\pi)^4 \delta(P+Q) \mathcal{G}_{k,\pi^a}^{-1}(P). \quad (5)$$

Here the four-momenta P and Q have a Matsubara frequency and the space momentum \vec{P} and \vec{Q} in the temporal and spatial components, respectively. The field variables are taken to be their ground state expectation values. $\mathcal{G}_{k,\sigma}(P)$ and $\mathcal{G}_{k,\pi^a}(P)$ converge on the temperature Green's functions for the respective mesons as $k \rightarrow 0$. The flow equations for $\mathcal{G}_{k,\sigma(\pi)}(P)$ ⁴ is obtained from the second derivatives of Eq. (1) with respect to the meson fields:

$$(2\pi)^4 \delta^{(4)}(P+Q) \partial_k \mathcal{G}_{k,\sigma}^{-1}(P) = \frac{1}{2} \frac{\delta^2}{\delta \sigma(P) \delta \sigma(Q)} \left[\frac{\partial_k R_k}{\Gamma_k^{(2)} + R_k} \right] \Big|_{\Phi=\Phi_0}, \quad (6)$$

$$(2\pi)^4 \delta^{(4)}(P+Q) \partial_k \mathcal{G}_{k,\pi^a}^{-1}(P) = \frac{1}{2} \frac{\delta^2}{\delta \pi^a(P) \delta \pi^a(Q)} \left[\frac{\partial_k R_k}{\Gamma_k^{(2)} + R_k} \right] \Big|_{\Phi=\Phi_0}. \quad (7)$$

Equations (6) and (7) contain the third and fourth derivatives of EAA in the right-hand side. The flow equation for $\Gamma_k^{(n)}$ contains $\Gamma_k^{(n+1)}$ and $\Gamma_k^{(n+2)}$ leading to an infinite hierarchy of a coupled equation, and thus it is difficult to obtain the exact solution of Eq. (1) in general. Therefore some approximations are needed to reduce the infinitely coupled differential equations to a solvable form. In the present work, we are interested in the low-energy modes around the critical point, which in turn play the dominant role for the determination of the phase structure around there. Thus we take so-called the local potential approximations where only the leading order in the derivative expansion of the meson fields is considered and the wave-function renormalization is neglected, and assume the following form for the EAA in the present work [23]:

$$\Gamma_k [\bar{\psi}, \psi, \phi] = \int_0^{\frac{1}{T}} d\tau \int d^3x \left\{ \bar{\psi} (\not{\partial} + g_s(\sigma + i\vec{\pi} \cdot \vec{\pi}\gamma_5) - \mu\gamma_0) \psi + \frac{1}{2}(\partial_\mu\phi)^2 + U_k(\phi^2) - c\sigma \right\}, \quad (8)$$

where $U_k(\phi^2)$ is the scale-dependent potential (effective potential) for the mesons.

The analytic continuation of the Green's function can be performed in the flow equation by making use of three-dimensional regulators which do not depend on frequency [19, 20, 24, 25]. We adopt the three-dimensional forms of the so-called optimized regulators, proposed by Litim [26]:

$$R_k^B(\vec{q}) = (k^2 - \vec{q}^2) \theta(k^2 - \vec{q}^2), \quad (9)$$

$$R_k^F(\vec{q}) = i\vec{q} \left(\sqrt{\frac{k^2}{\vec{q}^2}} - 1 \right) \theta(k^2 - \vec{q}^2). \quad (10)$$

Here, $R_k^B(\vec{q})$ and $R_k^F(\vec{q})$ are the regulators for bosons and fermions, respectively.

With the above regulators and assumptions of the uniform condensation of σ field and no π condensate in the ground state,

⁴ From now on we consider only isospin symmetric case and abbreviate the

isospin index for pions.

$\sigma_0 = \langle \sigma \rangle$ and $\langle \vec{\pi} \rangle = 0$, the flow equation for U_k reads [23]:

$$\partial_k U_k(\sigma^2) = \frac{k^4}{12\pi^2} \left[-2N_f N_c \left[\frac{1}{E_\psi(\sigma)} \tanh \frac{E_\psi(\sigma) + \mu}{2T} + \frac{1}{E_\psi(\sigma)} \tanh \frac{E_\psi(\sigma) - \mu}{2T} \right] + \frac{1}{E_\sigma(\sigma)} \coth \frac{E_\sigma(\sigma)}{2T} + \frac{3}{E_\pi(\sigma)} \coth \frac{E_\pi(\sigma)}{2T} \right], \quad (11)$$

where

$$E_a(\sigma) := \sqrt{k^2 + M_a^2(\sigma)}, \quad (12)$$

for $a = \psi, \sigma, \pi$, and $M_a(\sigma)$ is defined as follows:

$$M_\psi(\sigma) := g_s \sigma, \quad (13)$$

$$M_\sigma^2(\sigma) := \frac{\partial^2 U_k}{\partial \sigma^2}, \quad (14)$$

$$M_\pi^2(\sigma) := \frac{1}{\sigma} \frac{\partial U_k}{\partial \sigma}. \quad (15)$$

After solving the flow equation, the σ condensate σ_0 is determined from the minimum of the effective potential $U_{k \rightarrow 0}$:

$$\sigma_0 = \arg \min_{\sigma} (U_{k \rightarrow 0}(\sigma^2) - c\sigma). \quad (16)$$

The flow equations of the temperature Green's function (6) and (7) can be evaluated with U_k and σ_0 . The analytic continuation of $\mathcal{G}_{k,\sigma(\pi)}(P)$ by the replacement $iP^0 \rightarrow \omega + i\epsilon$ for the Matsubara frequency with ϵ being a positive infinitesimal number give the scale-dependent retarded Green's functions $G_{k,\sigma(\pi)}^R(\omega, \vec{p})$, which are to converge on the retarded Green's functions for the mesons as $k \rightarrow 0$: The flow equations for $G_{k,\sigma(\pi)}^R(\omega, \vec{p})$ now read [19, 20]:

$$\partial_k G_{k,\sigma}^R(\omega, \vec{p})^{-1} = \left[J_{k,\sigma\sigma}(P) (\Gamma_{k,\sigma\sigma\sigma}^{(0,3)})^2 + 3J_{k,\pi\pi}(P) (\Gamma_{k,\sigma\pi\pi}^{(0,3)})^2 - \frac{1}{2} I_{k,\sigma}^{(2)} \Gamma_{k,\sigma\sigma\sigma\sigma}^{(0,4)} - \frac{3}{2} I_{k,\pi}^{(2)} \Gamma_{k,\sigma\sigma\pi\pi}^{(0,4)} - 2N_c N_f J_{k,\bar{\psi}\psi}^{(\sigma)}(P) \right]_{iP^0 \rightarrow \omega+i\epsilon}, \quad (17)$$

$$\partial_k G_{k,\pi}^R(\omega, \vec{p})^{-1} = \left[J_{k,\sigma\pi}(P) (\Gamma_{k,\sigma\pi\pi}^{(0,3)})^2 + J_{k,\pi\sigma}(P) (\Gamma_{k,\sigma\pi\pi}^{(0,3)})^2 - \frac{1}{2} I_{k,\sigma}^{(2)} \Gamma_{k,\sigma\sigma\pi\pi}^{(0,4)} - \frac{5}{2} I_{k,\pi}^{(2)} \Gamma_{k,\pi\pi\tilde{\pi}\tilde{\pi}}^{(0,4)} - 2N_c N_f J_{k,\bar{\psi}\psi}^{(\pi)}(P) \right]_{iP^0 \rightarrow \omega+i\epsilon}. \quad (18)$$

Here, $\tilde{\pi}$ denotes a pion field with a isovector component different from π . $J_{k,\alpha\beta}(P)$, $I_{k,\alpha}^{(2)}$ and $J_{k,\bar{\psi}\psi}^{(\alpha)}(P)$ ($\alpha, \beta = \sigma, \pi$) are defined as

$$J_{k,\alpha\beta}(P) := T \sum_{Q^0} \int \frac{d^3 \vec{q}}{(2\pi)^3} \partial_k R_k^B(\vec{q}) G_{k,\alpha}^B(P)^2 G_{k,\beta}^B(Q - P), \quad (19)$$

$$I_{k,\alpha}^{(2)} := T \sum_{Q^0} \int \frac{d^3 \vec{q}}{(2\pi)^3} \partial_k R_k^B(\vec{q}) G_{k,\alpha}^B(Q)^2, \quad (20)$$

$$J_{k,\bar{\psi}\psi}^{(\alpha)}(P) := T \sum_{Q^0} \int \frac{d^3 \vec{q}}{(2\pi)^3} \text{tr} \left[\Gamma_{\bar{\psi}\psi\alpha}^{(2,1)} G_{k,\bar{\psi}\psi}^F(Q) \partial_k R_k^F(\vec{q}) G_{k,\bar{\psi}\psi}^F(Q) \Gamma_{\bar{\psi}\psi\alpha}^{(2,1)} G_{k,\bar{\psi}\psi}^F(Q - P) \right], \quad (21)$$

where $G_{k,\alpha}^B(Q)$ and $G_{k,\bar{\psi}\psi}^F(Q)$ are defined as

$$G_{k,\alpha}^B(Q) := \left[Q^2 + M_\alpha^2(\sigma_0) + R_k^B(\vec{q}) \right]^{-1}, \quad (22)$$

$$G_{k,\bar{\psi}\psi}^F(Q) := \left[Q^2 - \mu\gamma_0 + M_\psi(\sigma_0) + R_k^F(\vec{q}) \right]^{-1}. \quad (23)$$

We refer to Appendix A of Ref. [15] for more practical expressions of Eqs. (19)–(21) after the Matsubara summation. Note, that in our truncation, the meson propagator (22) in the flow equation depends on the scale-dependent meson screening mass (14)–(15). We will discuss some features of the resultant spectral function owing to this approximation in Sec. III D.

The three- and four-point functions $\Gamma_{\bar{\psi}\psi\phi_i}^{(2,1)}$, $\Gamma_{k,\phi_i\phi_j\phi_l}^{(0,3)}$, and $\Gamma_{k,\phi_i\phi_j\phi_l\phi_m}^{(0,4)}$ are defined as

$$\left. \frac{\delta}{\delta\phi_i(P_1)} \frac{\delta}{\delta\bar{\psi}(P_2)} \Gamma_k \frac{\delta}{\delta\psi(P_3)} \right|_{\Phi=\Phi_0} = (2\pi)^4 \delta^{(4)}(P_1 + P_2 + P_3) \Gamma_{\bar{\psi}\psi\phi_i}^{(2,1)}, \quad (24)$$

$$\left. \frac{\delta^3\Gamma_k}{\delta\phi_i(P_1)\delta\phi_j(P_2)\delta\phi_l(P_3)} \right|_{\Phi=\Phi_0} = (2\pi)^4 \delta^{(4)}(P_1 + P_2 + P_3) \Gamma_{k,\phi_i\phi_j\phi_l}^{(0,3)}, \quad (25)$$

$$\left. \frac{\delta^4\Gamma_k}{\delta\phi_i(P_1)\delta\phi_j(P_2)\delta\phi_l(P_3)\delta\phi_m(P_4)} \right|_{\Phi=\Phi_0} = (2\pi)^4 \delta^{(4)}(P_1 + P_2 + P_3 + P_4) \Gamma_{k,\phi_i\phi_j\phi_l\phi_m}^{(0,4)}. \quad (26)$$

The initial conditions of the flow equations are specified at the UV scale $k = \Lambda$ from the bare action (2):

$$U_\Lambda(\phi^2) = \frac{1}{2}m_\Lambda^2\phi^2 + \frac{1}{4}\lambda_\Lambda(\phi^2)^2, \quad (27)$$

$$G_{\Lambda,\sigma(\pi)}^R(\omega, \vec{p})^{-1} = \omega^2 - \vec{p}^2 - M_{\sigma(\pi)}^2(\sigma_0^2)|_{k=\Lambda}. \quad (28)$$

Before closing the section, we briefly describe our numerical implementations. We use the grid method to solve Eq. (11). Thus higher powers of ϕ^2 in U_k are automatically incorporated. As pointed out in Ref. [15], the grid intervals $\Delta\sigma$ and Δt for σ and $t = \exp(k)$, respectively, should satisfy a condition to maintain numerical instability in the evolution of the flow. We fix $\Delta\sigma = 0.32$ MeV and set Δt so that the condition is satisfied. We introduce an IR cutoff $k = k_{\text{IR}}$ at which the evolution is stopped because the stability condition makes the calculation time-consuming beyond that scale. In practice, k_{IR} is set to be smaller than 3 MeV in our calculation. The calculation is expected to be reliable for the analysis of modes with greater momentum scale than k_{IR} . The positive infinitesimal ϵ in the replacement of the frequency is set to $\epsilon = 1$ MeV.

III. NUMERICAL RESULTS AND DISCUSSIONS

In this section, we first show how the parameters in our model are determined with a special attention to the current quark mass since our EAA does not explicitly contain the current quark mass term; the explicit breaking of chiral symmetry is given by the last term $-c\sigma$ in the action. Then we proceed to show the numerical results on the phase diagram and the spectral properties of the low-energy modes with the current quark mass being varied.

A. Parameter setting

We first show the physical parameters which reproduce the empirical value of the pion mass in the vacuum [15, 19, 20]. The parameter values and resultant values of some observables in the vacuum are shown in Table I, where m_{con} and

$m_{\sigma(\pi)}$ are defined as follows:

$$m_{\text{con}} = M_\psi(\sigma_0)|_{k \rightarrow 0}, \quad (29)$$

$$m_{\sigma(\pi)} = M_{\sigma(\pi)}(\sigma_0)|_{k \rightarrow 0}. \quad (30)$$

For analyzing the cases with various current quark masses, we vary the parameter c which represents the effect of explicit breaking of the chiral symmetry in our model and can be related to the current quark mass m_q , as shown below: Other parameters such as Λ , m_Λ , λ_Λ and g_s are fixed to the values listed in Table I. The classical relation between σ and $\bar{\psi}\psi$ is given by the variation of Eq. (2) with respect to σ . Neglecting the kinematic term and the high-order terms of σ , one finds

$$\sigma \sim -\frac{g_s}{m_\Lambda^2} \bar{\psi}\psi. \quad (31)$$

Substituting Eq. (31) into Eq. (2), the current quark mass can be read off from the quark mass term $-(cg_s/m_\Lambda^2)\bar{\psi}\psi$ as

$$m_q \sim \frac{cg_s}{m_\Lambda^2}. \quad (32)$$

The values of c and the corresponding m_q as well as the meson masses are listed in Table II. We note that the Gell-Mann–Oakes–Renner (GOR) relation gives the almost the same quark masses.

B. Positions of critical points

In this subsection, we determine the position of the critical point in the (T, μ) -plane for each current mass. We remark that for determination of the phase structure with the critical point being identified, we need to calculate the *sigma* condensate $\sigma_0 = \langle\sigma\rangle$ for a wide region of the (T, μ) -plane.

O(4) critical line; chiral limit

In the case of the chiral limit, the chiral transition is of a second order at finite temperature for vanishing or small μ . Thus the critical line, i.e., an O(4) critical line exists in the high-temperature and low-density region starting from a point

TABLE I. Parameter set for the physical vacuum.

Λ	m_Λ/Λ	λ_Λ	c/Λ^3	g_s	σ_0	m_{con}	m_π	m_σ
1000 MeV	0.794	2.00	0.00175	3.2	93 MeV	286 MeV	137 MeV	496 MeV

TABLE II. Explicit breaking parameter c explored in this work and corresponding particle masses from Eq. (32)

c/Λ^3	0	0.00025	0.0005	0.00075	0.001	0.00125	0.0015	0.00175	0.002	0.003
m_q [MeV]	0	1.27	2.54	3.81	5.08	6.35	7.61	8.88	10.15	15.23
m_π [MeV]	0	54	76	92	105	117	127	137	146	175
m_σ [MeV]	111	336	390	423	448	467	483	496	508	546

TABLE III. The position of the Z_2 critical point $(T_c(m_q), \mu_c(m_q))$ for each m_q .

m_q [MeV]	1.27	2.54	3.81	5.08	6.35	7.61	8.88	10.15	15.23
$T_c(m_q)$ [MeV]	8.6	7.7	6.9	6.3	5.9	5.5	5.1	4.8	4.0
$\mu_c(m_q)$ [MeV]	264.3059	268.8192	272.8095	276.5925	280.2998	283.7038	286.8499	289.9452	301.4115

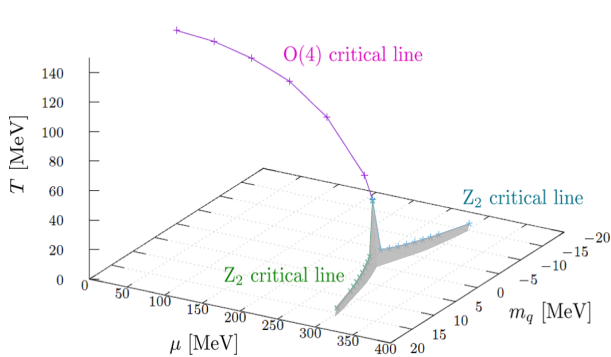


FIG. 1. The calculated phase structure in the (T, μ, m_q) -space with the O(4) and Z_2 critical lines being identified. The shaded area indicates that the phase transition is first order there. The phase diagram for the fictitious case with $m_q < 0$ is also shown: The phase structure is symmetric with respect to the $m_q = 0$ plane because the theory is invariant under the transformation $m_q \rightarrow -m_q$ and global phase transformations of fields. As mentioned in Sec. I, such a wing-like structure is common to various systems which have a tricritical point [8–10, 13].

$(T \neq 0, \mu = 0)$. The O(4) critical line terminates at the tricritical point where it is connected to the first-order phase transition line in the high-density and low-temperature region. To specify the phase boundary, we search the points where σ_0 changes from 0 to a nonzero value in the (T, μ) -plane. Then, we examine whether a gap in σ_0 appears or not to distinguish the order of the phase transition. Around the tricritical point, we calculate σ_0 with changing the chemical potential with an interval of 0.0001 MeV for each temperature with 1 MeV intervals. A gap of σ_0 is found to appear at $T = 44$ MeV, but does not appear at $T = 45$ MeV. Thus we conclude that a first-order phase transition at $T = 44$ MeV and the tricritical point between 44 MeV and 45 MeV. The location of the O(4) critical line is depicted in Fig. 1 in which the Z_2 lines for finite m_q are also shown; see below.

For $m_q \neq 0$, the phase transition becomes of crossover in the lower-chemical potential region while the first-order phase transition line persists in the high chemical potential region. At the endpoint of the first-order phase transition line, the phase transition is of second order, and accordingly the screening mass m_σ^2 , which is the inverse of the chiral susceptibility, vanishes. This critical point is called the Z_2 critical point. To locate the Z_2 critical point $(T_c(m_q), \mu_c(m_q))$, we search the point where m_σ takes the smallest value by varying T and μ with an interval of $\Delta T = 0.1$ MeV and $\Delta\mu = 0.0001$ MeV, respectively. We also confirmed that the phase change is of crossover at temperatures above the Z_2 critical temperature $T_c(m_q)$ and of first-order at temperatures below $T_c(m_q)$, by investigating the gap of σ_0 . The location of the Z_2 critical point for each m_q is depicted in Fig. 1, and the sets of values of $(T_c(m_q), \mu_c(m_q))$ for each m_q are shown in Table III. One finds that as m_q becomes larger, the critical point shifts to the low-temperature and high chemical potential region.

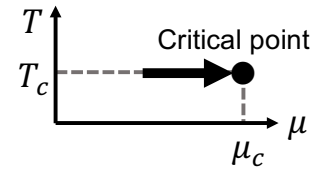


FIG. 2. A schematic view on how to approach a critical point in our calculations. The temperature is fixed to the critical temperature $T_c(m_q)$ and the chemical potential μ approaches the critical chemical potential $\mu_c(m_q)$ from the region $\mu < \mu_c(m_q)$.

TABLE IV. Decay and absorption processes in the sigma and pion channels and their kinematic constraints. σ^* and π^* represent virtual particles in the sigma and pion channels, respectively. ω and \vec{p} are the energy and momentum of the virtual particles. α represents σ and π .

Channel	Process	Constraint
Sigma meson	$\sigma^* \rightarrow \alpha\alpha$	$\omega \geq \sqrt{\vec{p}^2 + (2m_\alpha)^2}$
	$\sigma^* \rightarrow \bar{\psi}\psi$	$\omega \geq \sqrt{\vec{p}^2 + (2m_{\text{con}})^2}$
	$\sigma^*\alpha \rightarrow \alpha$	$\omega \leq \vec{p} $
	$\sigma^*\psi \rightarrow \psi$	$\omega \leq \vec{p} $
Pion	$\pi^* \rightarrow \sigma\pi$	$\omega \geq \sqrt{\vec{p}^2 + (m_\sigma + m_\pi)^2}$
	$\pi^* \rightarrow \bar{\psi}\psi$	$\omega \geq \sqrt{\vec{p}^2 + (2m_{\text{con}})^2}$
	$\pi^*\sigma \rightarrow \pi$	$\omega \leq \sqrt{\vec{p}^2 + (m_\pi - m_\sigma)^2} \theta(m_\pi - m_\sigma)$
	$\pi^*\pi \rightarrow \sigma$	$\omega \leq \sqrt{\vec{p}^2 + (m_\sigma - m_\pi)^2} \theta(m_\sigma - m_\pi)$
	$\pi^*\psi \rightarrow \psi$	$\omega \leq \vec{p} $

C. Behavior of low-energy modes around the critical points

In this section, we show the results of the spectral functions $\rho_{\sigma,\pi}$ in the mesonic channels, almost exclusively focusing on that in the sigma channel ρ_σ ; we discuss the behavior of low-energy modes around the critical points when the current quark mass is varied.

Before entering into the results, we list up the possible physical processes which may give rise to a peak or bump in the spectral functions $\rho_{\sigma,\pi}$ as preliminaries [15]. In addition to one-particle modes of the mesons, decay and absorption processes of the excitation modes cause a peak or bump in the spectral functions. The decay and absorption processes together with the respective kinematic conditions in the sigma and pion channels are shown in Table IV. In particular, the process $\sigma^*\psi \rightarrow \psi$ denotes a collisional process of the virtual σ state with quarks, which leads to (quark) particle-hole (p-h) excitations of a phonon type. This is the so-called Landau damping and is known to play an essential role to make the specific soft mode at the Z_2 critical point [13].

Now that we have finished the preliminaries, we show how the properties of the low-energy excitations in the scalar channel as extracted from the spectral function as μ approaches the critical chemical potential $\mu_c(m_q)$ from below at fixed temperature $T = T_c(m_q)$ for each current quark mass; see Fig. 2. A remark is in order here: For $m_q \neq 0$, $M_\sigma^2(\sigma_0)$ tends to take a negative value which causes numerical instability at some small k during the flow when $\mu > \mu_c$, and we restrict ourselves to the cases with μ smaller than the critical value.

We consider the spectral function not only vanishing momentum but also finite \vec{p} . Note that spectral functions depend only on $p = |\vec{p}|$, since the system is isotropic.

Appearance of tachyonic mode at physical quark mass

For the sake of the self-containedness, we begin with showing the numerical result for the physical quark mass $m_q = 8.88$ MeV, which is essentially the same as that presented in the previous paper [15] but with a slightly better preci-

sion. Figure 3(a) displays the spectral functions $\rho_\sigma(\omega, p)$ at $p = 50$ MeV for a few values of the chemical potential close to μ_c at $T = T_c$. For smaller μ , a peak and bumps are present in the time-like region, whereas a bump in the space-like region is seen; the peak in the time-like region represents the σ mesonic mode, while the bump in the space-like region denotes p-h excitations due to the coupling between the scalar and vector channels $\langle \bar{\psi}\psi \bar{\psi}\psi \rangle$ at finite μ . A notable point is that the σ meson peak sitting in the time-like region goes down to lower energy as μ is increased toward μ_c and eventually penetrates into the space-like region $\omega < p$ as the system is quite close to the critical point. This behavior can be more effectively seen in the contour $\rho_\sigma(\omega, p)$ mapped onto (ω, p) -plane: Fig. 3(b) displays the downward shift of the peak and the resultant anomalous dispersion relation in which the group velocity of the σ mode exceeds the speed of light. Admittedly, it might be caused by the possible violation of the causality owing to the use of the three-dimensional regulator⁵, and thus it would be desirable to check the regulator dependence [27, 28]. However, it should be noted that the superluminal group velocity seems to appear only in the limited situations, contrary to what is expected by the regulator origin. Another possibility is that a level repulsion between σ and 2σ modes causes the appearance of this tachyonic mode as pointed out in Ref. [15]. In fact, Fig. 3(a) shows that the well-defined 2σ threshold energy moves down so that the level repulsion with the σ mesonic mode becomes more effective.

The physical meaning of the appearance of the tachyonic mode: analysis with varying quark mass

In the previous work [15], the physical significance and the origin of the appearance of the tachyonic mode were, unfortunately, not pursued but left for a future work. Now we deal with this task. First of all, we notice that the σ -to- 2σ coupling gets to exist due to the explicit violation of chiral symmetry dictated by the current quark mass m_q . Therefore it should be intriguing to examine the behavior of the spectral function for smaller m_q leading to a suppressed σ -to- 2σ coupling.

Figure 4 shows the case of a finite but tiny quark mass, $m_q = 1.27$ MeV. Both figures show a downward shift of the peak of the sigma mesonic mode and accordingly of the 2σ threshold energy, while a bump due to the p-h excitations is clearly seen in the space-like region as in the case of $m_q = 8.88$ MeV. Nevertheless, no anomalous behavior with a superluminal group velocity appears in the dispersion relation.

Figure 5 shows the case when m_q is slightly increased to $m_q = 3.81$ MeV. Although the anomalous dispersion relation has yet to appear, one sees a non-monotonic peak shift in the spectral function. The peak first moves down as in the smaller m_q case (the first and second panels from the left in (b)), but turns upward for larger μ (the third panel), then moves down

⁵ We thank J. Pawłowski for pointing out this possibility

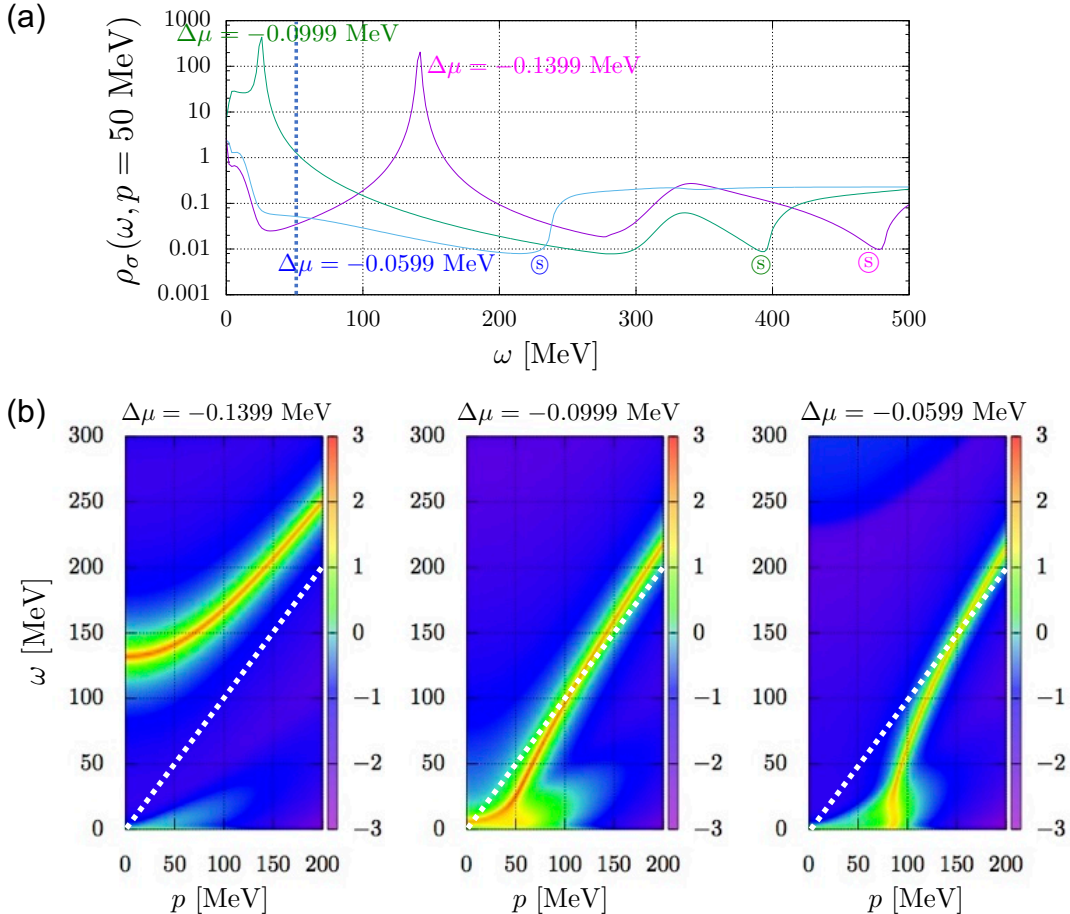


FIG. 3. Spectral functions ρ_σ in the scalar channel near the Z_2 critical point for the physical quark mass, $m_q = 8.88$ MeV. The temperature is fixed at T_c and the chemical potential is increased with an interval $\Delta\mu = \mu - \mu_c$. (a) The spectral functions $\rho_\sigma(\omega, p)$ at $p = 50$ MeV. The dotted vertical line (in blue) shows the energy $\omega = p$ on the light cone, while \circledcirc indicates the threshold energy of the 2σ mode. (b) The contour maps of ρ_σ (in logarithmic scale) in the (ω, p) -plane for the same temperature and the chemical potentials as those in (a). The dotted straight line (in white) denotes the light-cone $\omega = p$.

again (the fourth panel) as the system further approaches the critical point. Although such a change should be the result of the competing and μ -dependent level repulsions of the σ mesonic mode with the low-lying p-h excitations and high-lying 2σ bump, it is admittedly not so easy to give a clear account of such a non-monotonic behavior of the dispersion curve. Nevertheless, the group velocity of any modes do not become superluminal for this case.

The situation changes when $m_q = 5.08$ MeV as shown in Fig. 6: The σ peak in the low momentum region is pushed down to the space-like region. As the σ mode in the high-momentum region remains time-like, the resultant dispersion relation exhibits a superluminal group velocity and hence the anomalous tachyonic behavior appears, as was the case for the physical quark mass.

D. Discussion

Penetration of the sigma mode into space-like momentum region

In the previous work [15], we pointed out that the level repulsion between σ and 2σ modes causes the downward shift of the sigma mesonic mode by demonstrating that the three-point vertex of sigma $\Gamma_{k,\sigma\sigma\sigma}^{(0,3)}$, which gives rise to the level repulsion, strongly affects the energy shift of the sigma mesonic mode. The downward shift of these modes at physical quark mass can be found in Fig. 3(a).

In the chiral limit, $\Gamma_{k,\sigma\sigma\sigma}^{(0,3)}$ vanishes on the O(4) critical line because the symmetry under the transformation $\sigma \rightarrow -\sigma$ exists. Thus the level repulsion owing to finite $\Gamma_{k,\sigma\sigma\sigma}^{(0,3)}$ does not happen in the chiral limit. At finite but small current quark masses, $\Gamma_{k,\sigma\sigma\sigma}^{(0,3)}$ on the Z_2 critical line is expected to slowly increase as m_q increases, as schematically shown in Fig. 7. Consequently, the level repulsion is weakened by the small coupling at small current quark masses. This finding is consistent

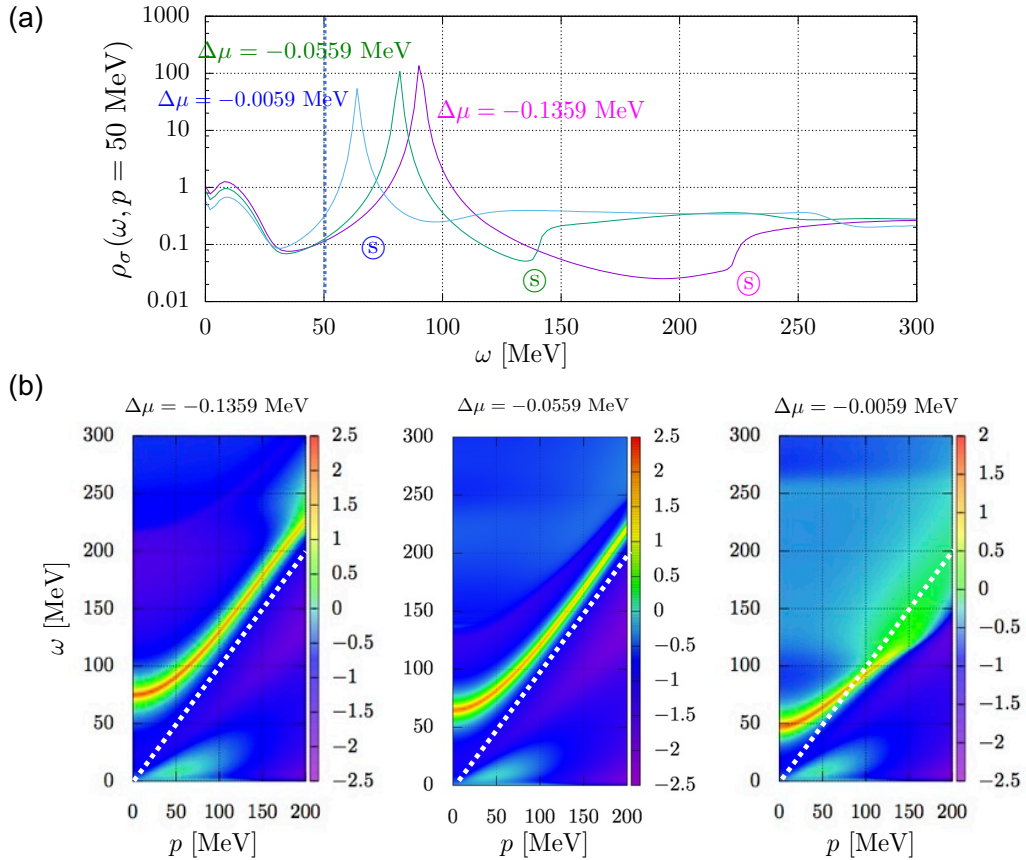


FIG. 4. The same as Fig. 3, but for $m_q = 1.27$ MeV. The temperature is fixed to $T_c(m_q) = 8.6$ MeV.

with the absence of the penetration of the sigma mode into the space-like momentum region, despite the strong downward shift of the 2σ mode.

For larger m_q , the group velocity of the sigma mesonic mode is superluminal for small but finite momenta at μ close to but below $\mu_c(m_q)$. One of the possibilities is that such an appearance of the tachyonic mode simply shows that the system is unstable, i.e., the ground state or the equilibrium state we have assumed is not the true one in these situations. A clue may be given by the fact that the tachyonic behavior as well as the softening itself in the sigma channel occur at finite momenta. Recently it has been suggested that the chiral inhomogeneous phase may exist so that it reveals the first-order phase transition line between the hadronic phase and the quark-gluon plasma phase [29–32]. In the present work, we have taken it for granted that the sigma condensate σ_0 is homogeneous with vanishing pion condensate in the equilibrium. Thus our result might indicate that the system is to undergo a phase transition to a state with an inhomogeneous sigma condensate near the Z_2 critical point at μ smaller than μ_c at small and vanishing temperature; as is shown below, any anomalous behavior is not seen for the excitation modes in the pion channel.

Soft modes at the critical point

Before closing this section, we discuss the systematic view of the soft modes on the $O(4)$ and Z_2 critical lines on the basis of the results given above. Figure 8 shows the contour map of ρ_σ near the $O(4)$ critical point $(T, \mu) = (45$ MeV, 260.3599 MeV) on the $O(4)$ critical line nearby the tricritical point. One sees a clear ridge in the time-like momentum region ($\omega > p$) as can be described by a dispersion relation $\omega_\sigma(p)$, which is an isoscalar one-particle mode, i.e., the sigma mesonic mode. As the system approaches the critical point, $\omega_\sigma(p)$ moves down toward zero energy, strongly in the lower-momentum region and eventually almost touches the zero energy for vanishing momenta. Thus one sees that Fig. 8 beautifully shows that the sigma mesonic mode is the soft mode of the $O(4)$ critical point.

At finite but small quark mass $m_q = 1.27$ MeV for instance, one finds the downward shift of the peak, which does not, however, reach $\omega = 0$ even at the immediate vicinity of the critical point, as shown in Fig. 9. Thus the sigma meson is not a soft mode at the Z_2 critical point. This picture is consistent with the arguments of Ref. [13, 14]. A remark is in order here: The dispersion curve of the sigma mesonic mode in the right panel of Fig. 4(b) and Fig. 9 penetrates into the space-like momentum region in the high-momentum region.

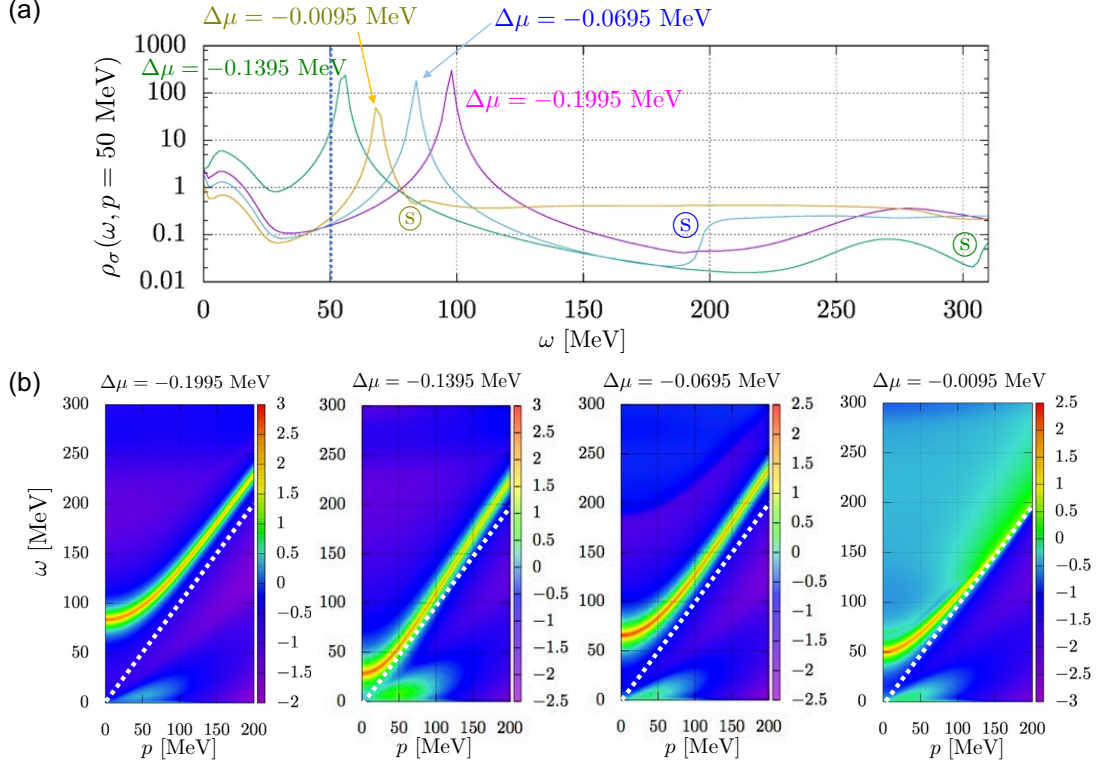


FIG. 5. The same as Fig. 4, but for $m_q = 3.81$ MeV. The temperature is fixed to $T_c(m_q) = 6.9$ MeV.

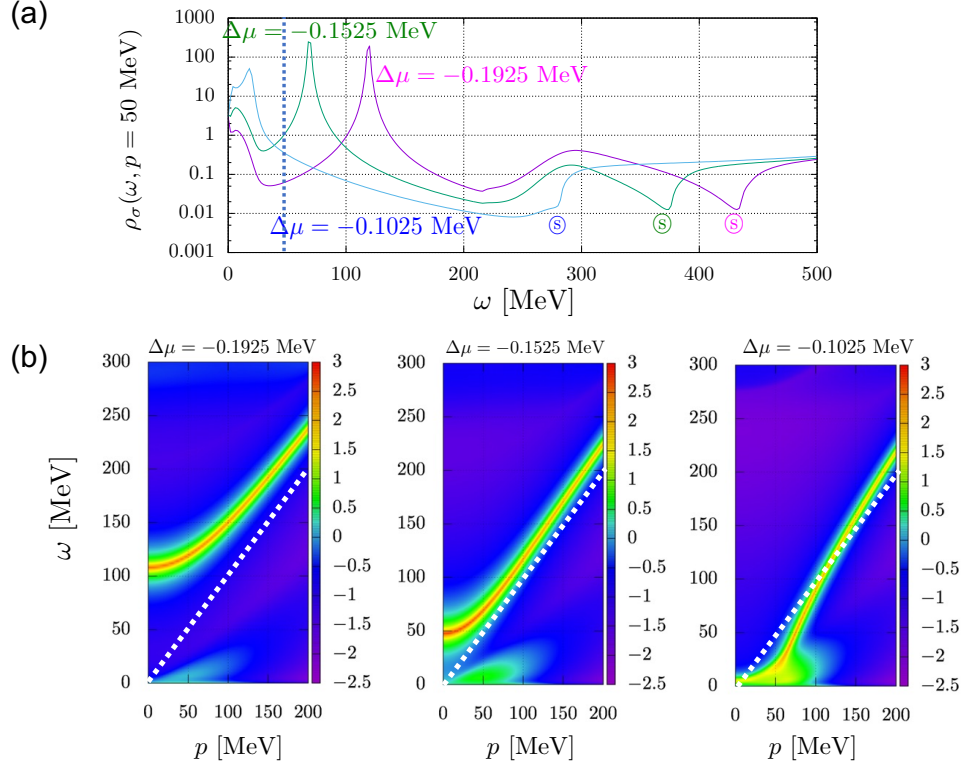


FIG. 6. The same as Fig. 4, but for $m_q = 5.08$ MeV. The temperature is fixed to $T_c(m_q) = 6.3$ MeV.

This anomalous and would-be interesting behavior is, how-

ever, can be an artifact largely caused by our approximation in

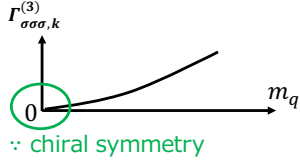


FIG. 7. 3-point vertex $\Gamma_{k,\sigma\sigma\sigma}^{(0,3)}$ on the Z_2 critical line as a function of m_q .

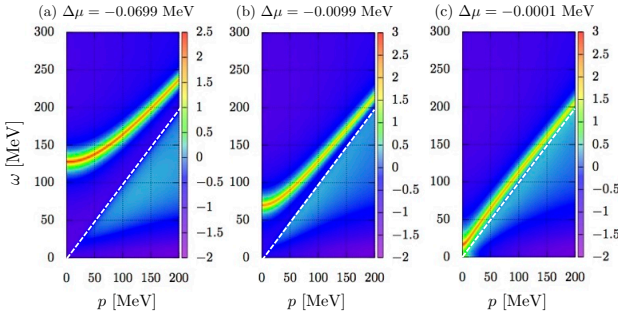


FIG. 8. The contour map of ρ_σ (in logarithmic scale) near the O(4) critical point at $(T, \mu) = (45 \text{ MeV}, 260.3599 \text{ MeV})$. The temperature is fixed to 45 MeV. Here $\Delta\mu = \mu - 260.3599 \text{ MeV}$ is the relative position from the O(4) critical point. The dotted straight line (in white) denotes the light-cone $\omega = p$.

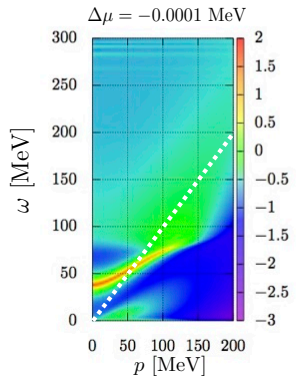


FIG. 9. The same as Fig. 4, but for $\Delta\mu = -0.0001 \text{ MeV}$.

contrast to the tachyonic behavior seen in the low-momentum region for larger m_q . First of all, we note that since the σ propagator is approximated in terms of the k -dependent screening mass $M_\sigma(\sigma_0)$ as given by Eq. (22), the threshold of the 2σ mode is also necessarily given by the (physical) screening mass $m_\sigma = M_\sigma(\sigma_0)|_{k \rightarrow 0}$, and hence the 2σ threshold at momentum p does not coincide with the twice of the σ -peak energy at momentum $p/2$: For instance, when $m_q = 8.88 \text{ MeV}$ and μ is not too close to μ_c , as seen by $\Delta\mu = -0.1399 \text{ MeV}$ in Fig. 3(a), the 2σ threshold ($\simeq 480 \text{ MeV}$) is larger than $2\omega_\sigma^{\text{peak}}(p/2) \simeq 260 \text{ MeV}$. This larger 2σ threshold in the present calculation implies that the level repulsion between the σ - 2σ modes is underestimated. Thus, the tachyonic behavior seen in the present work should persist in the exact treatment where a stronger level repulsion can be expected.

This is also the case with $m_q = 5.08 \text{ MeV}$. However, when μ is as close to μ_c as given by $\Delta\mu = -0.0001 \text{ MeV}$, the screening mass m_σ almost vanishes and accordingly the threshold energy of the 2σ mode is greatly underestimated and given by $\omega \sim p$, which would act to push down $\omega_\sigma(p)$ at the high momentum region owing to the level repulsion. Then it in turn leads to the penetration of $\omega_\sigma(p)$ into the space-like momentum region at high momenta.

When the current quark mass is further increased, the sigma mesonic mode can move down to $\omega = 0$, but it is accompanied with the appearance of the tachyonic mode, which may indicate the existence of a true ground state such as inhomogeneous chiral condensate, as emphasized above.

We also investigate the spectral function in the pion channel. In the chiral limit, we obtain the dispersion relation of the pion in the broken phase as $\omega = p$, which is consistent with the fact that pions become Nambu-Goldstone modes. At finite current quark mass, the dispersion relation of the pion mode is found to hardly change near the Z_2 critical points and does not show any critical behavior, in contrast to the case of the sigma channel.

IV. SUMMARY

We have explored possible character change of the low-energy modes in the scalar channels around the QCD critical point with varying the current quark mass m_q to elucidate the physical meaning of the anomalous behavior of the sigma mesonic and associated particle-hole modes found in our previous work [15]: For this purpose, we have calculated the spectral functions in the mesonic channels as well as the thermodynamic quantities using the functional renormalization group (FRG) method with the 2-flavor quark-meson model for varied quark masses.

In the first part, we have given the complete and quantitative phase structure focusing on the change of the nature and the location of the critical point in the three-dimensional space (T, μ, m_q) consisting of temperature T , quark chemical potential μ and m_q , as shown in Fig. 1: In the chiral limit, the chiral transition is of second order for vanishing or relatively smaller μ , and the critical points form an O(4) critical line until the tricritical point at which the phase transition turns to a first order for larger μ . For a finite m_q , the phase change is crossover for vanishing and small μ and then the Z_2 critical line extends from the tricritical point.

We have shown the spectral function $\rho_\sigma(\omega, p)$ as a function of ω for some p and also given the contour map of $\rho_\sigma(\omega, p)$ for whole (p, ω) plane in the low energy region extracted from $\rho_\sigma(\omega, p)$; the contour map clearly exhibits the dispersion relations (curves) of the sigma mesonic mode and particle-hole (phonon) mode as a ridge or bump of the contour, and thereby clarified how the spectral properties of the low-energy modes in the sigma channel are changed as μ approaches the critical chemical potential from below with T being fixed at T_c for each current quark mass.

At the physical current quark mass $m_q = 8.88 \text{ MeV}$ reproducing the empirical value of the pion in vacuum, the dis-

persion relation $\omega_\sigma(p)$ of the sigma mesonic mode moves down and penetrates into and stay in the space-like region ($\omega < p$) in the low-momentum regime slightly *before* the system reaches the critical point: Such a drastic downward shift of the dispersion relation necessarily makes the sigma mesonic mode superluminal at finite momenta, as was found in the previous paper [15].

Although one might suspect that the existence of such a superluminal mode could be an artifact due to the violation of the causality owing to the use of the three-dimensional regulator, the present analysis tracing the spectral change of the scalar mode with varying current quark mass has shown that it has a physical origin. First of all, the downward shift can be understood in terms of the level repulsion between the sigma and the two-sigma mode [15] and this effect is suppressed for small m_q and vanishes in the chiral limit because the three-point vertex of the sigma $\Gamma_{k,\sigma\sigma\sigma}^{(0,3)}$ vanishes on the critical line due to the chiral symmetry. Our analysis with smaller m_q shows the absence of the superluminal velocity for such m_q : Indeed at as small as $m_q = 1.27$ MeV, $\omega_\sigma(p)$ does not penetrate into the space-like momentum region in the low-momentum region and no superluminal mode appears, although $\omega_\sigma(p)$ moves down toward the low-energy region as the system approaches the critical point. For $m_q = 3.81$ MeV, the dispersion curve of the sigma mesonic mode shows a non-monotonic behavior as the system approaches the critical point, but does not show any superluminal behavior. For $m_q \geq 5.08$ MeV, the dispersion curve is further pushed down before it moves up and the downward shift makes the sigma mesonic mode superluminal as at $m_q = 8.88$ MeV. These results strongly suggest that the strong downward shift of $\omega_\sigma(p)$ leading to the appearance of the tachyonic mode with a superluminal velocity has a definite physical origin due to the σ - 2σ coupling caused by the explicit breaking of chiral symmetry by the current quark mass. It should be emphasized that the tachyonic dispersion relation appears when μ is close to but smaller than the critical value μ_c . A natural interpre-

tation of the appearance of the tachyonic mode at *finite momenta* is that the assumed equilibrium state is unstable against a new state with an inhomogeneous σ condensate prior to the Z_2 critical point where the phonon mode mainly composed of particle-hole excitations would overwhelm the σ mesonic sector [13, 14].

Incidentally, on the O(4) critical line for the chiral limit, the dispersion relation $\omega_\sigma(p)$ of the sigma mesonic mode moves down toward zero energy at $p = 0$ MeV, which means that the sigma mesonic mode is the soft mode of the O(4) critical point. On the Z_2 critical line at finite but small quark mass, $m_q = 1.27$ MeV for instance, $\omega_\sigma(p)$ never touch the zero energy near the critical point, which is in accordance with the fact that the sigma mesonic mode is not the soft mode of the Z_2 critical point [13, 14].

The present analysis on the excitation modes admittedly only suggests the possibility that the high-density matter undergoes a phase transition to an inhomogeneous state. To have a definite answer of the new state, it is necessary to develop methods to deal with non-uniform equilibrium states in the framework of FRG. This is a challenging task and left as a future work.

ACKNOWLEDGMENTS

T. Y. was supported by the Grants-in-Aid for JSPS fellows (Grant No. 16J08574). T. K. was supported by JSPS KAKENHI Grants (Nos. 16K05350 and 15H03663) and by the Yukawa International Program for Quark-Hadron Sciences (YIPQS). K.M. was supported by JSPS Grant 16K05349, the Grants-in-Aid for Scientific Research on Innovative Areas from MEXT (Grant No. 24105008) and National Science Center, Poland under grants:, Maestro DEC-2013/10/A/ST2/00106. He also acknowledges support from RIKEN iTHES group. Numerical computation in this work was carried out at the Yukawa Institute Computer Facility.

-
- [1] F. R. Brown, F. P. Butler, H. Chen, N. H. Christ, Z. Dong, W. Schaffer, L. I. Unger, and A. Vaccarino, Phys. Rev. Lett. **65**, 2491 (1990).
- [2] R. D. Pisarski and F. Wilczek, Phys. Rev. **D29**, 338 (1984).
- [3] K. I. Ishikawa, Y. Iwasaki, Y. Nakayama, and T. Yoshie, “Nature of chiral phase transition in two-flavor QCD,” (2017), arXiv:1706.08872 [hep-lat].
- [4] A. Tomya, G. Cossu, S. Aoki, H. Fukaya, S. Hashimoto, T. Kaneko, and J. Noaki, “Evidence of effective axial U(1) symmetry restoration at high temperature QCD,” (2016), arXiv:1612.01908 [hep-lat].
- [5] M. Asakawa and K. Yazaki, Nucl. Phys. **A504**, 668 (1989).
- [6] A. Barducci, R. Casalbuoni, S. De Curtis, R. Gatto, and G. Pettini, Phys. Lett. **B231**, 463 (1989).
- [7] A. Barducci, R. Casalbuoni, S. De Curtis, R. Gatto, and G. Pettini, Phys. Rev. **D41**, 1610 (1990).
- [8] J. Kogut and M. Stephanov, *The Phases of Quantum Chromodynamics: From Confinement to Extreme Environments*, Cambridge Monographs on Particle Physics, Nuclear Physics and Cosmology (Cambridge University Press, 2010).
- [9] R. B. Griffiths, Phys. Rev. B **7**, 545 (1973).
- [10] W. Gebhardt and U. Krey, *Phasenübergänge und kritische Phänomene: Eine Einführung für Physiker im Hauptstudium* (Friedrich Vieweg, 1980).
- [11] T. Kunihiro, Phys. Lett. **B271**, 395 (1991).
- [12] T. Kunihiro, in *Quantum chromodynamics and color confinement. Proceedings, International Symposium, Confinement 2000, Osaka, Japan, March 7-10, 2000* (2000) pp. 287–295, arXiv:hep-ph/0007173 [hep-ph].
- [13] H. Fujii and M. Ohtani, Phys. Rev. **D70**, 014016 (2004), arXiv:hep-ph/0402263 [hep-ph].
- [14] D. T. Son and M. A. Stephanov, Phys. Rev. **D70**, 056001 (2004), arXiv:hep-ph/0401052 [hep-ph].
- [15] T. Yokota, T. Kunihiro, and K. Morita, PTEP **2016**, 073D01 (2016), arXiv:1603.02147 [hep-ph].
- [16] J. Berges, N. Tetradis, and C. Wetterich, Phys. Rept. **363**, 223 (2002), arXiv:hep-ph/0005122 [hep-ph].

- [17] J. M. Pawłowski, Annals Phys. **322**, 2831 (2007), arXiv:hep-th/0512261 [hep-th].
- [18] H. Gies, *ECT* School on Renormalization Group and Effective Field Theory Approaches to Many-Body Systems Trento, Italy, February 27-March 10, 2006*, Lect. Notes Phys. **852**, 287 (2012), arXiv:hep-ph/0611146 [hep-ph].
- [19] R.-A. Tripolt, N. Strodthoff, L. von Smekal, and J. Wambach, Phys. Rev. **D89**, 034010 (2014), arXiv:1311.0630 [hep-ph].
- [20] R.-A. Tripolt, L. von Smekal, and J. Wambach, Phys. Rev. **D90**, 074031 (2014), arXiv:1408.3512 [hep-ph].
- [21] C. Wetterich, Phys. Lett. **B301**, 90 (1993).
- [22] A. A. Abrikosov, L. P. Gorkov, I. Dzyaloshinskii, and R. A. Sil'verman, *Methods of quantum field theory in statistical physics* (Dover, New York, NY, 1975).
- [23] B.-J. Schaefer and J. Wambach, Nucl. Phys. **A757**, 479 (2005), arXiv:nucl-th/0403039 [nucl-th].
- [24] K. Kamikado, N. Strodthoff, L. von Smekal, and J. Wambach, Eur. Phys. J. **C74**, 2806 (2014), arXiv:1302.6199 [hep-ph].
- [25] S. Floerchinger, JHEP **05**, 021 (2012), arXiv:1112.4374 [hep-th].
- [26] D. F. Litim, Phys. Rev. **D64**, 105007 (2001), arXiv:hep-th/0103195 [hep-th].
- [27] J. M. Pawłowski and N. Strodthoff, Phys. Rev. **D92**, 094009 (2015), arXiv:1508.01160 [hep-ph].
- [28] N. Strodthoff, Phys. Rev. **D95**, 076002 (2017), arXiv:1611.05036 [hep-th].
- [29] E. Nakano and T. Tatsumi, Phys. Rev. **D71**, 114006 (2005), arXiv:hep-ph/0411350 [hep-ph].
- [30] D. Nickel, Phys. Rev. **D80**, 074025 (2009), arXiv:0906.5295 [hep-ph].
- [31] D. Nickel, Phys. Rev. Lett. **103**, 072301 (2009), arXiv:0902.1778 [hep-ph].
- [32] D. Müller, M. Buballa, and J. Wambach, Phys. Lett. **B727**, 240 (2013), arXiv:1308.4303 [hep-ph].